LETTER Communicated by Timm Lochmann

Approximate, Computationally Efficient Online Learning in Bayesian Spiking Neurons

Levin Kuhlmann
levink@unimelb.edu.au
NeuroEngineering Laboratory, Department of Electrical and Electronic Engineering, The University of Melbourne, and the Centre for Neural Engineering, The University of Melbourne, Victoria 3010, Australia

Michael Hauser-Raspe
michael.hauser-raspe@cantab.net
MARCS Institute, University of Western Sydney, Penrith, Australia

Jonathan H. Manton
jonathan.manton@gmail.com
Control and Signal Processing Laboratory, Department of Electrical and Electronic Engineering, The University of Melbourne, Victoria 3010, Australia

David B. Grayden
grayden@unimelb.edu.au
NeuroEngineering Laboratory, Department of Electrical and Electronic Engineering, The University of Melbourne, and the Centre for Neural Engineering, The University of Melbourne, Victoria 3010, Australia

Jonathan Tapson
j.tapson@uws.edu.au
André van Schaik
a.vanschaik@uws.edu.au
MARCS Institute, University of Western Sydney, Penrith, Australia

Bayesian spiking neurons (BSNs) provide a probabilistic interpretation of how neurons perform inference and learning. Online learning in BSNs typically involves parameter estimation based on maximum-likelihood expectation-maximization (ML-EM) which is computationally slow and limits the potential of studying networks of BSNs. An online learning algorithm, fast learning (FL), is presented that is more computationally efficient than the benchmark ML-EM for a fixed number of time steps as the number of inputs to a BSN increases (e.g., 16.5 times faster run times for 20 inputs). Although ML-EM appears to converge 2.0 to 3.6 times faster than FL, the computational cost of ML-EM means that ML-EM takes longer to simulate to convergence than FL. FL also provides reasonable

convergence performance that is robust to initialization of parameter estimates that are far from the true parameter values. However, parameter estimation depends on the range of true parameter values. Nevertheless, for a physiologically meaningful range of parameter values, FL gives very good average estimation accuracy, despite its approximate nature. The FL algorithm therefore provides an efficient tool, complementary to ML-EM, for exploring BSN networks in more detail in order to better understand their biological relevance. Moreover, the simplicity of the FL algorithm means it can be easily implemented in neuromorphic VLSI such that one can take advantage of the energy-efficient spike coding of BSNs.

1 Introduction

Bayesian inference provides an intuitive understanding of sensory, cognitive, and motor processing by describing these processes in probabilistic terms (Knill & Richards, 1996; Kording & Wolpert, 2004). In addition to the application of Bayesian inference to neural population models (Zemel, Dayan, & Pouget, 1998; Barber, Clark, & Anderson, 2003), more recently Bayesian inference has been applied at the level of single neurons in the form of Bayesian spiking neurons (BSNs) (Denève 2008a, 2008b; Lochmann & Denève, 2008). BSNs provide a probabilistic interpretation of how neurons can perform inference and learning, and BSN theory has been extended to provide explanations of sensory processing (Lochmann, Ernst, & Denève, 2012) and working memory (Boerlin & Denève, 2011). Learning in BSNs is local to a single neuron, meaning that BSNs can self-organize using only their inputs, although their organization is still constrained by underlying assumptions about how the inputs were generated. As a result of the self-organization of single BSNs, hierarchical feedforward networks of BSNs can generally be thought of as clustering systems. Moreover, BSN networks can be used to perform perceptual inference and learning in sensory networks, such as feature and object recognition, and this can be done using the efficient spike coding properties of BSNs. Specifically, "object" neurons at the top of a feedforward system that receive no supervisory signals can learn to connect to lower-level "feature" neurons that are simultaneously active when the object stimulus is present. In addition, lateral interactions can be used to activate different object neuron clusters when different object classes are present in order to allow clustered learning of object classes, where groups of few to many neurons could represent the presence or absence of different object classes. Although some BSN networks have been studied (Boerlin & Denève, 2011; Lochmann et al., 2012), learning in large feedforward, and potentially feedback, BSN networks has not yet been studied in detail.

Given that learning in BSNs involves maximum-likelihood expectation-maximization (ML-EM) (Denève, 2008b; Mongillo & Denève, 2008), learning is computationally intensive, and therefore it can be time-consuming to study networks of interesting complexity. Here, we present the fast learning (FL) algorithm, which increases the speed of learning in BSNs and should therefore make it easier to study the properties of networks of BSNs. The FL algorithm presented here is more robust and stable with respect to initialization of parameter estimates and a large set of true parameter combinations than an earlier version (Kuhlmann et al., 2012).

This letter is organized as follows. The methods are first presented, outlining the definition of a BSN, the new FL algorithm, and a benchmark ML-EM algorithm. In the results, the performance (parameter estimation accuracy and run time) of the FL algorithm and its dependence on various factors are explored. The FL and ML-EM algorithms are compared for a large number of true parameter combinations and for varied degrees in the uncertainty of the initial parameter estimates relative to the true parameter values. This is done in order to assess the robustness of the FL algorithm and highlight its strengths and weaknesses compared to ML-EM. We also consider the performance of FL in three-layer networks. It is worth noting that the FL and ML-EM algorithms are both online and adaptive, meaning that they can be applied to data in real time as they enter the system and that their parameter estimates will converge when the input statistics are stationary, but can adapt to estimate new parameter values if the input statistics change to a different stationary distribution.

2 Methods

2.1 Bayesian Spiking Neuron Equations. A BSN (Denève, 2008a, 2008b) is defined to have an explicit space and an implicit space (see Figures 1A and 1B). The explicit space represents the neuron, with N synaptic inputs indexed by i, input spike sequences s_t^i ($s_t^i = 1$ corresponds to the occurrence of a spike at time t on the ith synapse; otherwise $s_t^i = 0$), synaptic weights w_i, and output spike sequence O_t. The implicit space is defined by a two-state hidden Markov model (HMM), where the hidden state takes on values of $x_t = \{0, 1\}$ that, for example, model the presence or absence of a stimulus. When the hidden state is $x_t = 1$, it is considered "on" or "present," whereas when the hidden state is $x_t = 0$, it is considered "off" or "absent." The hidden states transition with the probabilities

$$P(x_t = d|x_{t-\Delta t} = c) = a_{cd} = \begin{bmatrix} (1 - r_{on}\Delta t) & r_{on}\Delta t \\ r_{off}\Delta t & (1 - r_{off}\Delta t) \end{bmatrix}, \tag{2.1}$$

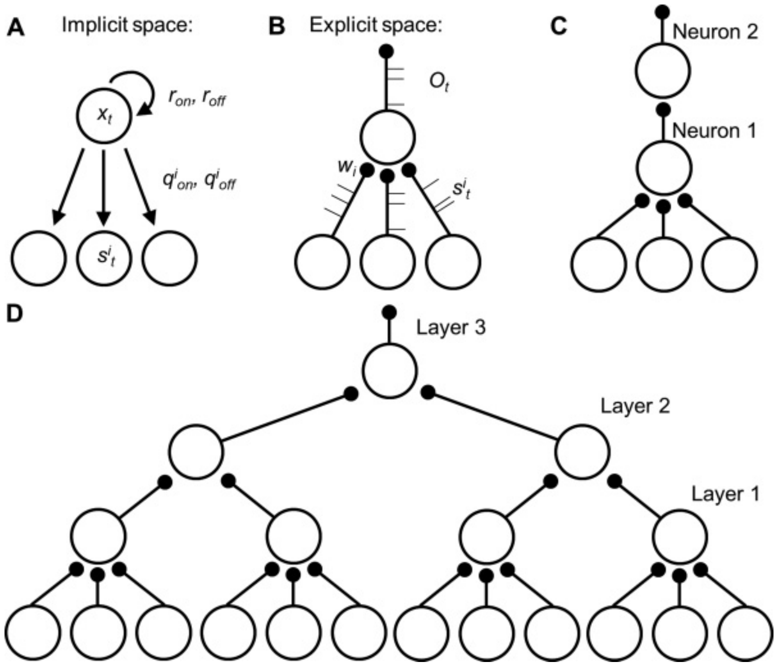

Figure 1: (A) The implicit space of a BSN involves a two-state HMM ($x_t = \{0,1\}$) that produces N independent outputs with two possible observations, and the outputs are indexed by i ($s^i_t = \{0,1\}$). The state transition rates are represented by r_{on} and r_{off}, and the observation rates are represented by q^i_{on} and q^i_{off}. (B) The explicit space of the BSN involves N synapses with weights w_i, the input spike sequences are assumed to be the outputs of the HMM ($s^i_t = \{0,1\}$), and the output spike sequence is given by O_t. (C) The simple two-neuron network studied in this letter. Neuron 1 receives $N = 20$ inputs derived from independent Poisson processes and provides the only input to neuron 2. (D) The small three-layer network studied in this letter. Each layer 1 neuron receives $N = 20$ inputs.

where r_{on} and r_{off} are the rates of *off* $\rightarrow$ *on* and *on* $\rightarrow$ *off* transitions, t is the current time, and Δt is the time step.

The HMM produces N independent observable outputs that can produce one of two observations within a time step, $s^i_t = \{0, 1\}$, where i indexes the N outputs. These N independent output observations of the HMM correspond to the inputs to the BSN and are modeled as inhomogeneous Poisson processes, where the process occurs as a homogeneous Poisson process either with rate q^i_{on} when $x_t = 1$ or with rate q^i_{off} when $x_t = 0$. For small time steps, the Poisson process can be described by a binomial process, and the observation probabilities for each synapse become

$$P(s_t^i = e|x_t = d) = b_{de}^i = \begin{bmatrix} (1 - q_{off}^i \Delta t) & q_{off}^i \Delta t \\ (1 - q_{on}^i \Delta t) & q_{on}^i \Delta t \end{bmatrix}. \tag{2.2}$$

For a BSN when the stimulus is either present or absent, the distribution of the number of output spikes per a given time interval matches closely a Poisson distribution (Denève, 2008a), and therefore it is possible to build hierarchies of BSNs. The aim of a single BSN is to code the log-odds ratio of the hidden state, x_t, in its output spikes. This is achieved by numerically integrating the differential equation of the log-odds ratio, L_t, along with a differential equation for the prediction of the log-odds ratio, G_t, which depends on the output spikes of the BSN. When the log-odds ratio goes above its prediction by $g_o/2$, an output spike is generated (represented by $O_t = 1$). This can be seen in the following equations (Denève, 2008a):

$$\Delta L_t = \left[r_{on}\left(1 + e^{-L_t}\right) - r_{off}\left(1 + e^{L_t}\right) - \theta_{th}\right]\Delta t + \sum_i w_i s_t^i, \tag{2.3}$$

$$\Delta G_t = \left[r_{on}\left(1 + e^{-G_t}\right) - r_{off}\left(1 + e^{G_t}\right)\right]\Delta t + g_o O_t, \tag{2.4}$$

$$O_t = \begin{cases} 1 & \text{iff } L_t > G_t + \frac{g_o}{2}, \\ 0 & \text{otherwise} \end{cases} \tag{2.5}$$

where

$$w_i = \log\left(\frac{q_{on}^i}{q_{off}^i}\right), \tag{2.6}$$

$$\theta_{th} = \sum_i \left(q_{on}^i - q_{off}^i\right), \tag{2.7}$$

and g_o is a free parameter that controls coding efficiency. Unless otherwise stated, for all simulations $g_o = 1.45$. Learning in a BSN involves estimation of the unknown parameters r_{on}, r_{off}, q_{on}^i, and q_{off}^i. Here, we compare learning with ML-EM and the FL algorithms. In what follows, the parameter estimates are denoted as $\hat{r}_{on}$, $\hat{r}_{off}$, $\hat{q}_{on}^i$, and $\hat{q}_{off}^i$, and θ and $\hat{\theta}$ denote the vectors of the parameters and the parameter estimates, respectively.

2.2 Benchmark ML-EM Algorithm. The benchmark online ML-EM algorithm is based on computing the sufficient statistics of the maximum likelihood function (Denève, 2008b; Mongillo & Denève, 2008). The algorithm converges to a local maximum if run for an adequate amount of time. Mongillo and Denève (2008) do not provide a proof of convergence for their online algorithm, although they explain that their online method converges to the same estimate as batch EM (Rabiner, 1989) for an appropriate discount factor and scheduling of parameter updates. For each time step, at time t, equations 2.8 to 2.11 are computed in the order presented. Equation 2.8 defines $\gamma^i_{cd}(s^i_t; \hat{\theta}(t-\Delta t))$, which is a weighting term that depends on the previous parameter estimates and determines the trajectories of the variables in equations 2.9 and 2.10,

$$\gamma^i_{cd}\big(s^i_t; \hat{\theta}(t-\Delta t)\big) = \frac{\hat{a}_{cd}(t-\Delta t)\hat{b}^i_{d,s^i_t}(t-\Delta t)}{\sum_{m,n} \hat{a}_{mn}(t-\Delta t)\hat{b}^i_{n,s^i_t}(t-\Delta t)Q^i_m(t-\Delta t)}, \tag{2.8}$$

where $\hat{\theta}(t-\Delta t)$ is the set of previous parameter estimates that determine the previous estimates of the transition, $\hat{a}_{cd}(t-\Delta t)$, and observation, $\hat{b}^i_{de}(t-\Delta t)$, probabilities as defined in equations 2.1 and 2.2, respectively. The variable $Q^i_l(t-\Delta t)$ represents the probability of being in state l at time t and is updated according to

$$Q^i_l(t) = \sum_m \gamma^i_{ml}\big(s^i_t; \hat{\theta}(t-\Delta t)\big)Q^i_m(t-\Delta t). \tag{2.9}$$

A statistic is then computed from which the current transition and observation probabilities can be estimated:

$$\begin{aligned}\varphi^{hi}_{cde}(t) = {}& \sum_l \gamma^i_{lh}\big(s^i_t; \hat{\theta}(t-\Delta t)\big) \times \big\{\varphi^{li}_{cde}(t-\Delta t) \\ &+ \eta\big[\delta\big(s^i_t - e\big)\delta(c-l)\delta(d-h)Q^i_l(t-\Delta t) - \phi^{li}_{cde}(t-\Delta t)\big]\big\},\end{aligned} \tag{2.10}$$

where η is a positive-valued temporal forgetting factor. The current transition and observation probabilities are given by

$$\hat{a}_{cd}(t) = \frac{\sum_{e,h,i} \phi^{hi}_{cde}(t)}{\sum_{d,e,h,i} \phi^{hi}_{cde}(t)}; \qquad \hat{b}^i_{de}(t) = \frac{\sum_{c,h} \phi^{hi}_{cde}(t)}{\sum_{c,e,h} \phi^{hi}_{cde}(t)}. \tag{2.11}$$

The BSN parameter estimates $\hat{r}_{on}$, $\hat{r}_{off}$, $\hat{q}^i_{on}$, and $\hat{q}^i_{off}$ can then be inferred from equations 2.1 and 2.2. The initialization and settings of the algorithm that were applied are $\phi^{hi}_{cde}(0) = 0$, $Q^i_1(0) = 0.5$, $\eta = 10^{-5}$. The statistic $\phi^{hi}_{cde}(t)$ is updated for the first 10^2 time steps without applying equation 2.11 so that it can stabilize. It should also be noted that this form of learning of the BSN directly depends on only the input spikes to the BSN and its parameters and not on any other variables of the BSN.

2.3 The Fast Learning Algorithm. As Denève (2008b), noted the parameters of the BSN (i.e., the transition rates and observation rates of the HMM) depend on the following intermediate statistics: the proportion of time spent in the *on* state, $\tau_{on}(t)$; the number of *on* $\rightarrow$ *off* transitions, $N_{on\rightarrow off}(t)$; the number of *off* $\rightarrow$ *on* transitions, $N_{off\rightarrow on}(t)$; the number of spikes occurring at the ith synapse during the *on* state, $N^i_{on}(t)$; and the number of spikes occurring at the ith synapse, $N^i(t)$. For each time step, the FL algorithm first estimates the hidden state from the log-odds ratio of the hidden state and then estimates these statistics in order to determine the parameters.

First, we note that the definition of the log-odds ratio of the hidden state, x_t, is

$$L_t = \log\left(\frac{P(x_t = 1|\mathbf{s}_{0\rightarrow t})}{P(x_t = 0|\mathbf{s}_{0\rightarrow t})}\right), \tag{2.12}$$

implying that the probability that the hidden state, x_t, is equal to 1 given the past synaptic inputs from all synapses that can be computed using

$$P(x_t = 1|\mathbf{s}_{0\rightarrow t}) = \frac{e^{L_t}}{1 + e^{L_t}}. \tag{2.13}$$

A robust way to determine if a hidden state transition has occurred is to set an auxiliary variable, $\tilde{x}_t$ (i.e. a hidden state estimate), such that

$$\tilde{x}_t = \begin{cases} 1 & \text{if } P(x_t = 1|\mathbf{s}_{0\rightarrow t}) > U_t \\ 0 & \text{if } P(x_t = 1|\mathbf{s}_{0\rightarrow t}) < D_t, \\ \tilde{x}_{t-\Delta t} & \text{otherwise} \end{cases} \tag{2.14}$$

where U_t and D_t are dynamic thresholds that depend on the maximum and minimum values of $P(x_t = 1|\mathbf{s}_{0\rightarrow t})$, respectively, over a window of length T:

$$U_t = \theta_U(M_t - m_t) + m_t, \tag{2.15}$$

$$D_t = \theta_D(M_t - m_t) + m_t, \tag{2.16}$$

with

$$M_t = \max\{P(x_u = 1|\mathbf{s}_{0\rightarrow u}) : u \in [t - \mathrm{T}, t]\}, \tag{2.17}$$

$$m_t = \min\{P(x_u = 1|\mathbf{s}_{0\rightarrow u}) : u \in [t - \mathrm{T}, t]\}, \tag{2.18}$$

and θ_U and θ_D are factors defining the position of the thresholds within the range of $P(x_t = 1|\mathbf{s}_{0\rightarrow t})$ over the last T seconds. These factors should be set such that $\theta_U > 0.5$ and $\theta_D < 0.5$ simply because $P(x_t = 1|\mathbf{s}_{0\rightarrow t})$ values above the midrange of $P(x_t = 1|\mathbf{s}_{0\to t})$ over the last T seconds best indicate x_t is likely to be 1, whereas $P(x_t = 1|\mathbf{s}_{0\to t})$ values below this midrange best indicate x_t is likely to be 0. In all simulations, T = 0.5 s. The dynamic thresholding is a heuristic method that provides a stability of estimation that cannot be achieved with static thresholds alone (such as by Kuhlmann et al., 2012). In particular, it ensures that state transitions can still be detected when transition rates are low, the number of input spikes is low, or the parameter estimates are far from the true parameter values.

An *on* → *off* transition variable is defined as

$$T_{off}(t) = \begin{cases} 1 & \text{if } \tilde{x}_t = 0 \text{ and } \tilde{x}_{t-\Delta t} = 1, \\ 0 & \text{otherwise} \end{cases} \tag{2.19}$$

and an *off* → *on* transition variable is defined as

$$T_{on}(t) = \begin{cases} 1 & \text{if } \tilde{x}_t = 1 \text{ and } \tilde{x}_{t-\Delta t} = 0. \\ 0 & \text{otherwise} \end{cases} \tag{2.20}$$

It is then possible to write update rules for the intermediate statistics respectively as follows:

$$\tau_{on}(t) = \eta\tilde{x}_t + (1-\eta)\tau_{on}(t-\Delta t), \tag{2.21}$$

$$N_{on\to off}(t) = \eta T_{off}(t) + (1-\eta)N_{on\to off}(t-\Delta t), \tag{2.22}$$

$$N_{off\to on}(t) = \eta T_{on}(t) + (1-\eta)N_{off\to on}(t-\Delta t), \tag{2.23}$$

$$N^i_{on}(t) = \eta s^i_t\tilde{x}_t + (1-\eta)N^i_{on}(t-\Delta t), \tag{2.24}$$

$$N^i(t) = \eta s^i_t + (1-\eta)N^i(t-\Delta t), \tag{2.25}$$

where each equation represents a moving average with exponential decay with a time constant τ and $\eta = \Delta t/(\Delta t + \tau)$ is a positive-valued forgetting factor. The forgetting factor η is present in both the FL and ML-EM algorithms. A small η means that learning/parameter estimation is smoother but also takes longer to converge. A large η means the algorithm forgets quickly but can also converge more quickly provided τ is of adequate duration to accurately estimate the intermediate statistics required to estimate the parameters.

The parameter estimates can then be calculated from equations 2.21 to 2.25 as follows:

$$\hat{r}_{on}(t) = \frac{N_{off\to on}(t)}{\Delta t(1-\tau_{on}(t))}, \tag{2.26}$$

$$\hat{r}_{off}(t) = \frac{N_{on\to off}(t)}{\Delta t(\tau_{on}(t))}, \tag{2.27}$$

$$\hat{q}^{i}_{on}(t) = \frac{N^{i}_{on}(t)}{\Delta t(\tau_{on}(t))}, \tag{2.28}$$

$$\hat{q}^{i}_{off}(t) = \frac{N^{i}(t) - N^{i}_{on}(t)}{\Delta t(1 - \tau_{on}(t))}. \tag{2.29}$$

In equations 2.26 and 2.29, it is important to note that the denominator includes 1 rather than the time constant of the online forgetting window, τ, and $\tau_{on}(t)$ represents a proportion of time rather than an actual time due to our normalized low-pass filter (see equations 2.21–2.25) and the use of a discrete time step, Δt.

The FL algorithm runs online by updating L_t using equation 2.3 and the previous parameter estimates. Then L_t is used in equation 2.13 to determine the auxiliary state estimate, $\tilde{x}_t$, in equation 2.14 which is needed to estimate the intermediate statistics in equations 2.21 to 2.25 via equations 2.15 to 2.20. From these statistics the current parameter estimates can be determined using equations 2.26 to 2.29. The current parameter estimates are then used to determine L_t in the next time step.

The FL algorithm is initialized by setting the intermediate statistics in equations 2.21 to 2.25 to zero and, as with the ML-EM algorithm, $\eta = 10^{-5}$. Moreover, the intermediate statistics were updated for the first 10^5 time steps without applying equations 2.26 to 2.29. In all simulations, the time step was set to $\Delta t = 0.1$ ms. To ensure numerical stability of the FL algorithm, it is important to prevent the observation rate estimates $\hat{q}^{i}_{on}$ and $\hat{q}^{i}_{off}$ from being very close to zero because this can cause the synaptic weights w_i to be undefined or to approach very large positive or negative numbers (as can be seen by inspecting equation 2.6). Moreover, during simulation, it is necessary to provide a small lower bound on the transition rate estimates $\hat{r}_{on}$ and $\hat{r}_{off}$ in order to prevent either parameter estimate from becoming too small and causing the log-odds ratio to grow very large in either the positive or negative direction, as the resting potential of the BSN corresponds to $\log(\hat{r}_{on}/\hat{r}_{off})$. This is especially important when a BSN receives only a small number of input spikes, which makes it harder to detect *off* $\to$ *on* and *on* $\to$ *off* transitions. In the simulations presented, the estimated transition and observation rates were forced to be above 0.1 s^{-1} and 10^{-3} s^{-1}, respectively. For similar reasons, the intermediate statistic, $\tau_{on}(t)$, was prevented from being zero by adding a small number, 10^{-15}, to this statistic.

The FL algorithm emulates the ML-EM algorithm in that it performs iterative online estimation of the state and the parameters, although ML-EM provides only a partial state estimate. In addition, there is no proven guarantee that the FL algorithm will converge on a fixed set of parameters. In contrast and as already mentioned, the ML-EM algorithm presented here converges to the same estimates as batch EM under certain conditions, although a general proof of convergence has not been published. Nevertheless, the computational simplicity of the FL algorithm means that it will be more computationally efficient than the ML-EM algorithm.

2.4 Computational Comparison of FL and ML-EM Algorithms. Here we explore online learning in a simple network with two BSNs where neuron 1 receives $N = 20$ Poisson process inputs and neuron 2 receives the output of neuron 1 as its only input (see Figure 1C). Many simulations of the FL algorithm were performed over a large set of true parameter values to give evidence that the FL algorithm converges reliably in the absence of convergence proofs. The performances of the FL and ML-EM algorithms are compared.

The online learning problem that is analyzed first involves simulation of the implicit space HMM of neuron 1. The simulated hidden state time series, which depends on r_{on} and r_{off}, reflects the presence or absence of a feature out in the world that the BSN response encodes. From the simulated hidden states, the simulated observations are produced and fed as input to neuron 1. When the hidden state is 1, the observations are simulated as a homogeneous Poisson process with rate q^i_{on}; when the hidden state is 0, the observations are simulated as a homogeneous Poisson process with rate q^i_{off}. Learning in neuron 1 then involves estimation of the parameters r_{on}, r_{off}, q^i_{on}, and q^i_{off}.

The output of a BSN is approximately Poisson (Denève, 2008a), and therefore the output of neuron 1 can be used as the only input to neuron 2. Note that the hidden state, x_t, is the same for neurons 1 and 2 because neuron 2 receives input only from neuron 1 and therefore will learn only the same state transition rates coded in the output of neuron 1. This is synonymous with a hierarchical causal generative HMM model with two states where the top state causes the bottom state (i.e., it follows the top state) and the bottom state produces the observations (Denève, 2008a). Neuron 2 is considered here to highlight some features of the FL algorithm in simple chain networks.

2.5 The FL Algorithm Applied to Three-Layer Networks. The FL algorithm is also applied to three-layer networks to explore parameter estimation and hidden state decoding accuracy of the FL algorithm across layers in a network. Two three-layer networks are considered—one small, one large. The small three-layer network has 4, 2, and 1 neurons in the first, second, and third layers, respectively (see Figure 1D), and each neuron in layer 1 receives 20 inputs. The large three-layer network is similar to the small network; however, it involves a doubling of the synaptic inputs to the higher layers. This second network has 16, 4, and 1 neurons in the first, second, and third layers, respectively. Learning is considered for a

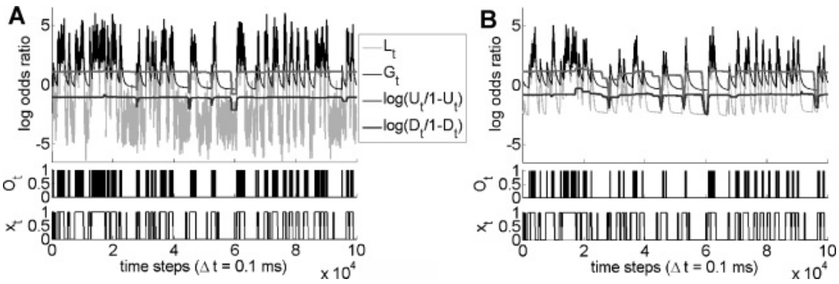

Figure 2: Example BSN simulations for (A) neuron 1 and (B) neuron 2 in the two-neuron network while running the FL algorithm. Each subfigure shows the last 10^5 time-steps of a 10^6 time-step simulation with $r_{on} = 8\ \mathrm{s}^{-1}$, $r_{off} = 10.5\ \mathrm{s}^{-1}$, and q^i_{on} and q^i_{off} uniformly selected in the range of 10 to 80 spikes/s for neuron 1. Initial parameter estimates were set to the true parameter values for neuron 1, while for neuron 2, initial transition rates were set to the same values as neuron 1. The initial observation rates for the single-input synapse to neuron 2 were set equal to the values of the first input synapse to neuron 1. In each neuron-specific subfigure, the top plot shows the log-odds ratio L_t, the prediction G_t, and the state transition thresholds, U_t and D_t, mapped onto the log-odds ratio axis. The middle plot shows the output spike sequence, O_t, and the lower plot shows the HMM state, x_t, unknown to the BSN. $g_o = 2$.

hierarchical causal generative HMM model where the top state corresponding to layer 3 causes the states corresponding to layer 2, which in turn cause the states corresponding to layer 1, and these bottom states produce the observations. BSN theory has been derived within the context of hierarchical causal models (Denève, 2008a); therefore, we restrict our study to these models.

3 Results

3.1 An Example Simulation Using FL. For the two-neuron network, Figure 2 shows an example simulation of neurons 1 and 2 while running the FL algorithm over 10^6 time steps. The time series that are shown correspond to the last 10^5 time steps of the simulation when the parameter estimates have stabilized. For both neurons, it can be seen that the log-odds ratio of the hidden state, L_t, and the output spike sequence, O_t, show a strong correlation with the hidden state, x_t. Moreover, there is less fluctuation in the log-odds ratio of neuron 2 than there is for neuron 1 because neuron 1 receives many more input spikes. Given this greater number of inputs, the output spikes of neuron 1 also provide a better representation of the hidden state.

3.2 FL Estimation Accuracy Depends on Various Factors. In addition to the BSN's free parameters, g_o and N (free in the sense that they are selected prior to running any algorithm), the FL algorithm introduces three free parameters to select before running the algorithm: the factors θ_U and θ_D, and the window length, T, used to define the dynamic thresholds. Based on simulations, a value of $T = 0.5$ s was empirically found to capture the range of state transition rates considered here, and therefore we focus our analysis on threshold factors θ_U and θ_D, the spiking threshold, g_o, and the range of true parameter values instead.

Based on equations 2.1 and 2.2 and given that a time step of 0.1 ms is used, the transition and observation rates should be limited to the range of 0 to 10^4 s^{-1}. For the two-neuron network, in simulations with FL, it was found that if the transition and observation rates covered the full range of 1–10^4 s^{-1} and $\theta_U = 0.75$ and $\theta_D = 0.25$, then the transition rates are significantly underestimated and the observation estimates are reasonably accurate (neuron 1 median estimation error values: r_{on}: −97.6%, r_{off}: −97.7%, q^i_{on}: 0.01%, q^i_{off}: −0.04%). Nevertheless, if we restrict ourselves to a physiologically plausible range of transition rates (1–115s^{-1}; these rates are adequate for capturing ecologically relevant changes of stimuli in the outside world) and observation rates (1–1000 s^{-1}; these rates span the allowed rates of neuronal spiking assuming a 1ms refractory period), we can achieve excellent average estimation performance as the remaining figures will show.

For the two-neuron network, Figures 3A to 3I show the sensitivity analysis of the FL algorithm for the threshold factors θ_U and θ_D for 100 simulations of 10^6 time steps with different true parameter combinations for each factor pair (i.e., (θ_U, θ_D)), with the true parameters lying in the physiologically plausible range. For each simulation, the initial parameter estimates were set to five times the values of the true parameters. It can be seen that the median estimation errors in r_{on} and r_{off} for neuron 1 (top row of Figures 3A and 3B) are quite varied, showing best performance away from low θ_U and high θ_D values, whereas the median error for q^i_{on} and q^i_{off} for neuron 1 (top row of Figures 3C and 3D) is minimally affected by the threshold factors with errors under about 1% for all factor pairs. The median errors in r_{on} and r_{off} for neuron 2 (top row of Figures 3E and 3F) show a similar sensitivity pattern to that seen for neuron 1, although errors are larger for neuron 2. These greater errors result from neuron 2 receiving fewer input spikes and therefore less information about state transitions. Note that sensitivity or error maps are not provided for q^i_{on} and q^i_{off} for neuron 2 because there are no true parameter values for this neuron to determine the error. The sign of the error or bias as a function of threshold factors θ_U and θ_D is captured in the bottom row of Figures 3A to 3F. Generally it can be seen that when the errors are large for r_{on} and r_{off} for both neurons 1 and 2, the bias tends to be positive (i.e., overestimation) and θ_U and θ_D are

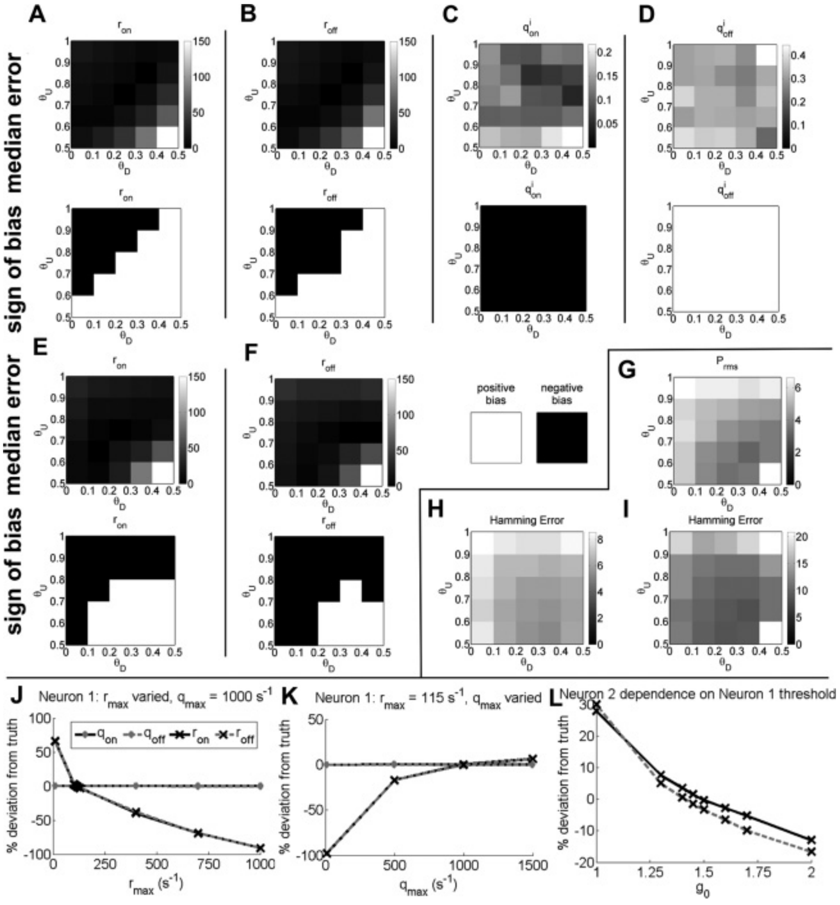

both closer to 0.5. For q^i_{on} and q^i_{off} of neuron 1, it can be seen that the bias is generally negative (i.e., underestimation) and positive, respectively.

For the same case as Figures 3A to 3F, Figure 3G demonstrates the median RMS error in the probability that the hidden state is 1, P_{rms}, as a function of the threshold factors for neuron 1. For a given 10^6 time step simulation, P_{rms} was computed over the last 10^5 time steps as the difference between the simulated $P(x_t = 1|\mathbf{s}_{0\to t})$ time series using the estimated parameters and the true parameters,

$$P_{rms} = 100\sqrt{\frac{1}{N_{rms}}\sum_{j=0}^{N_{rms}-1}\left(P(x_{t_j}=1|\mathbf{s}_{0\to t_j};\hat{\theta}(t_j)) - P(x_{t_j}=1|\mathbf{s}_{0\to t_j};\theta)\right)^2}, \tag{3.1}$$

where t_f is the end time of the simulation, $N_{rms} = 10^5$ is the number of time steps over which the RMS error is calculated, and $t_j = t_f - j\Delta t$. Moreover, Figures 3H and 3I show the percent Hamming error between the true and estimated hidden states as a function of the threshold parameters for neurons 1 and 2, respectively. Percent Hamming error was computed in a similar way to P_{rms} and was defined as

$$H = 100 \sqrt{\frac{1}{N_{rms}} \sum_{j=0}^{N_{rms}-1} |\tilde{x}_{t_j} - x_{t_j}|}, \tag{3.2}$$

where $t_j = t_f - j\Delta t$ also.

In Figures 3G to 3I, it can be seen that both P_{rms} and the percent Hamming error are lowest for factors θ_U and θ_D close to 0.75 and 0.25, respectively.

To assess how the true parameter value ranges affect parameter estimation, the maximum values for the range of the transition rates, $r_{\max}$, and the observation rates, $q_{\max}$, are varied within a physiologically plausible range in Figures 3J and 3K. In Figure 3J, it can be seen that if $q_{\max} = 1000\text{s}^{-1}$ and $r_{\max}$ is varied, then the transition rates are overestimated or underestimated if $r_{\max}$ is below or above 115 s^{-1}. In Figure 3K, it can be seen that if $r_{\max} = 115\text{s}^{-1}$ and $q_{\max}$ is varied, then the transition rates are underestimated

Figure 3: Estimation accuracy as a function of the dynamic threshold and the true parameter range for the FL algorithm for the two-neuron network. The median percent parameter estimation error (top row) and the corresponding sign of the error or bias (bottom row) plotted as functions of the dynamic threshold factors θ_U and θ_D for neuron 1 parameters (A) r_{on}, (B) r_{off}, (C) q^i_{on}, (D) q^i_{off}, and neuron 2 parameters (E) r_{on} and (F) r_{off}. The neuron 1 median RMS error of (G) $P(x_t = 1|\mathbf{s}_{0\to t})$, P_{rms}, (H) median percent Hamming error, H, and (I) neuron 2 median percent Hamming error, H, as functions of θ_U and θ_D. For each (θ_D, θ_U) pair, the median error was calculated over 100 simulations lasting 10^6 time steps for the 400% initial parameter perturbation case and, for neurons 1 and 2, r_{on} and r_{off} are uniformly selected in the range of 1 to 115 s^{-1}, and the q^i_{on} and q^i_{off} are uniformly selected in the range of 1 to 1000 spikes/s. To improve image clarity, the median state transition rate error was clipped at 150 s^{-1}. In the bias map legend, white indicates positive bias or overestimation and black indicates negative bias or underestimation for a given θ_U and θ_D pair. Median parameter estimation error of neuron 1 as a function of the true parameter range when (J) $r_{\max}$ is varied and the q^i_{on} and q^i_{off} are uniformly selected in the range of 1 to 1000 spikes/s and (K) $q_{\max}$ is varied and r_{on} and r_{off} are uniformly selected in the range of 1–115 s^{-1}. (L) Parameter estimation error of neuron 2 as a function of Neuron 1 threshold, g_o, for the same true parameter range as in panels A to I. The legend in panel J applies to panels K and L. For panels J–L, $\theta_U = 0.75$ and $\theta_D = 0.25$, and 1000 simulations were performed to obtain each median value.

or overestimated if $q_{\max}$ is below or above 1000 s^{-1}. Generally it was found that to minimize transition rate estimation error bias, one needs to have transition rates that are sufficiently lower than the observation rates, but not too low. Figures 3J and 3K also demonstrate that the median estimation error of the observation rates is always quite small and is independent of the true parameter range.

To assess the influence of the spiking threshold, g_o, in one layer on the estimation performance in the next layer, the spiking threshold for neuron 1 is varied for true parameter values corresponding to our physiologically plausible range; the estimation performance is plotted in Figure 3L. It can be seen that small and large values of neuron 1, g_o, lead to overestimation and underestimation of the transition rates for neuron 2, respectively, with an optimal value of around $g_o = 1.45$. Note that observation rate errors are not plotted because no true observation rates are defined for neuron 2. A low-spiking threshold value means more input spikes to neuron 2 and leads to too many false state transition detections, while a high-spiking threshold value leads to fewer input spikes and fewer true state transition detections.

In Figures 3J and 3K, it can generally be seen that the on and off observation rate estimation errors closely overlap each other, as do the on and off transition rate estimation errors in Figures 3J to 3L.

3.3 A Comparison Between FL and ML-EM for the Two-Neuron Network. For the two-neuron network, Figure 4 shows box whisker plots of the parameter estimation errors for the FL and ML-EM algorithms in cases where the initial parameter estimates were set to the true parameter values (0% initial parameter perturbation case) or the initial parameter estimates were set to five times the values of the true parameters (400% initial parameter perturbation case). Moreover, $\theta_U = 0.75$ and $\theta_D = 0.25$, and the true parameter values lie in our physiologically plausible range. Each case was simulated 1000 times for 10^6 time steps with different true parameter combinations each time. It can be seen that ML-EM performs the best for the 0% perturbation case, whereas for the 400% perturbation case, FL performs best for r_{on} and r_{off} and is comparable to ML-EM for q^i_{on} and q^i_{off}. The FL estimation errors do not change much between the 0% and 400% perturbation cases. We focus here on a fixed 400% initial parameter estimate perturbation because we are mostly interested in robustness and stability when the true parameters are varied over a large range. The behavior of FL for 0% and 400% initial parameter estimate perturbations is similar to that shown in Figure 3.

Figures 5A and 5B show that in terms of the percent Hamming error and P_{rms}, respectively, FL performs better than ML-EM for the 400% perturbation case, and increasing the number of time steps by a factor of 10 further improves the convergence of FL for the 400% perturbation case. ML-EM was simulated for only 10^6 time steps because the run time was too long. Moreover, for ML-EM, the P_{rms} is most meaningful, since

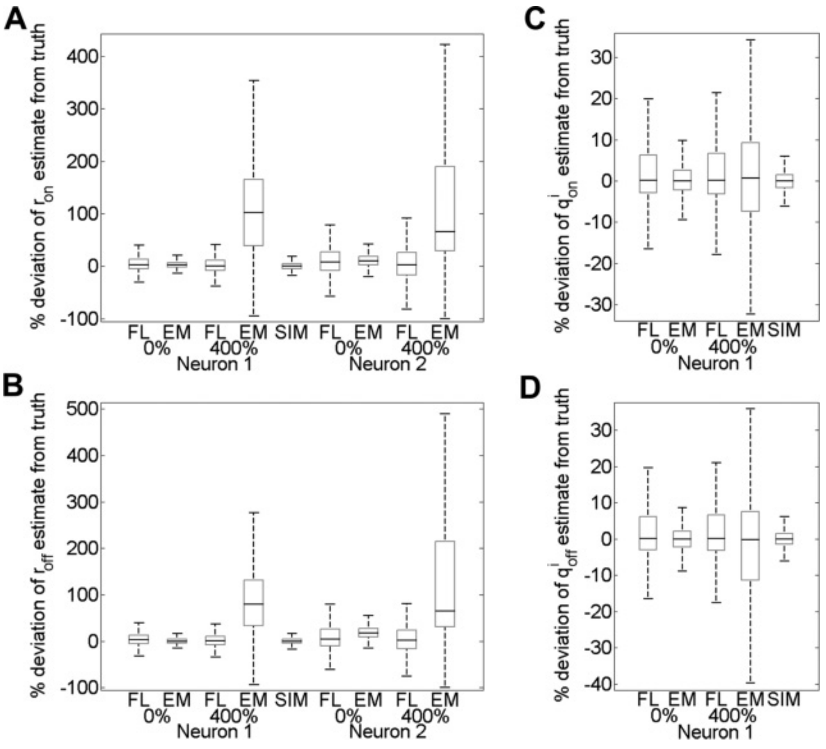

Figure 4: Comparison of parameter estimation performance between FL and ML-EM for the 0% and 400% initial parameter perturbation cases for the two-neuron network. The neuron 1 and neuron 2 distributions of percent parameter estimation error for (A) r_{on} and (B) r_{off}. The neuron 1 distributions of percent parameter estimation error for (C) q^i_{on} and (D) q^i_{off}. For each FL and EM case, data were collected over 1000 simulations lasting 10^6 time steps, where for neurons 1 and 2, r_{on} and r_{off} are uniformly selected in the range of 1 to 115 s^{-1}, and the q^i_{on} and q^i_{off} are uniformly selected in the range of 1 to 1000 spikes/s. To gauge the HMM simulation errors resulting from finite simulation times, the SIM distributions in panels A–D show the percent error of the parameters calculated from the hidden state, x_t, known to us but not the BSN, as well as the observations, s^i_t. In each box whisker the gray box bounds the 25th and 75th percentiles of the data, the black horizontal line represents the median, and the black dashed whiskers span the extreme points within 1.5 times the interquartile range.

the percent Hamming error values for ML-EM should be considered only approximate. This is because ML-EM gives only a partial state estimate, the probability $P(x_t = 1|\mathbf{s}_{0\rightarrow t})$, which needs to be thresholded (threshold set to 0.5) in order to obtain a nonoptimal state estimate used to compute the percent Hamming error.

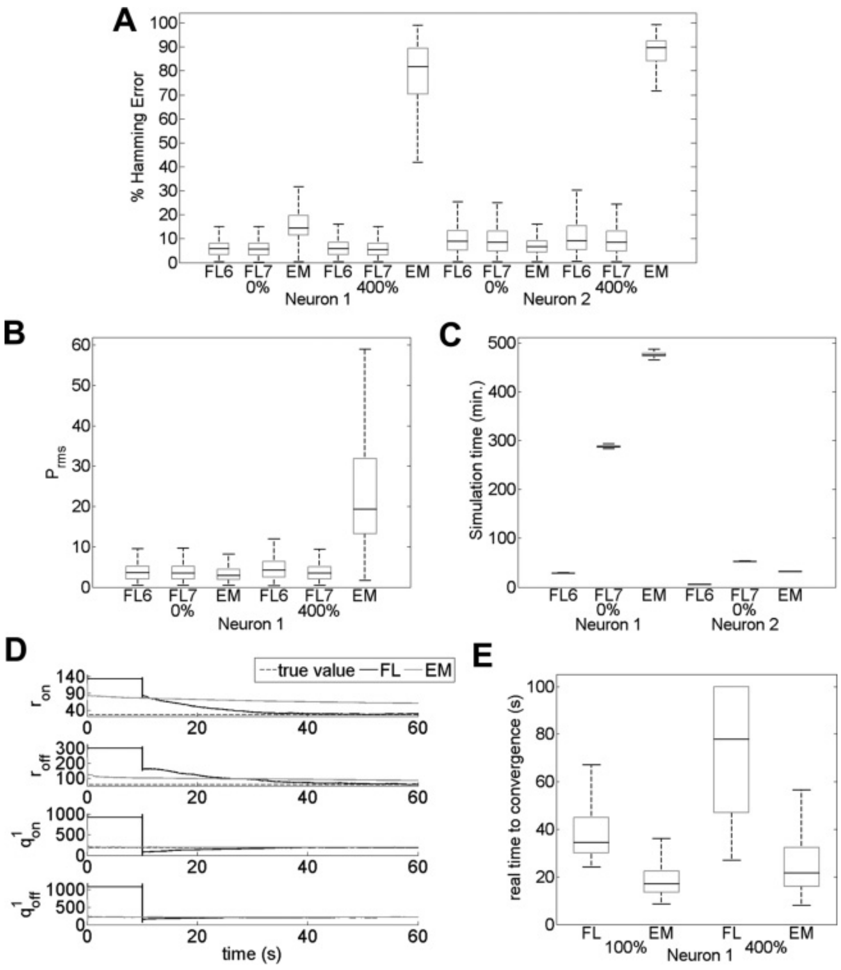

Figure 5: Estimation accuracy, computation time, and time to convergence in the two-neuron network. Comparison between FL and ML-EM for (A) % Hamming error distributions for neurons 1 and 2, (B) P_{rms} distributions for neuron 1, and (C) run-time distributions for neurons 1 and 2 for the 0% and 400% initial parameter perturbation cases. FL6 and FL7 refer to FL simulations involving 10^6 and 10^7 time steps, respectively. EM refers to EM simulations involving 10^6 time steps. (D) Example of parameter estimation evolution for neuron 1 for both FL (solid black) and ML-EM (solid gray) when the estimates begin 400% above the true parameter values. The dashed gray line indicates the true parameter values. (E) Distributions of the real time to convergence for the FL and ML-EM algorithms for neuron 1 for 100% and 400% initial parameter perturbation cases. For (E) all simulations lasted 10^6 time steps (100 s). For panels A–E, simulation settings and box whisker details are the same as for Figure 4.

Figure 5C captures the median run times for the FL and ML-EM algorithms applied to neurons 1 and 2 simulated for 10^6 time steps over 1000 different true parameter value combinations in the 0% initial parameter estimate perturbation case. For neuron 1, FL is approximately 16.5 times more computationally efficient than ML-EM for a 20-synapse BSN. For neuron 2, FL is approximately 6.1 times more computationally efficient than ML-EM for a 1-synapse BSN. These results indicate that FL becomes more computationally efficient than ML-EM as the number of synapses, and also the number of input spikes to a BSN increases. Note also that for neuron 1, simulating FL for 10^7 time steps still results in run times nearly less than half the time required for ML-EM to run 10^6 time steps.

The "real" time (seconds of synaptic input) convergence properties of FL and ML-EM are summarized in Figures 5D and 5E. Figure 5D shows an example of parameter estimation for neuron 1 when the initial parameter estimates are 400% above the true values. The parameter estimates are held constant for the first 10^5 and 10^2 time steps for FL and ML-EM, respectively, in order to let the intermediate statistics stabilize. FL estimates then converge close to the true values for all parameters (note that only r_{on}, r_{off}, q^1_{on}, and q^1_{off} are shown), while the ML-EM estimates converge close to the true values for all the observation rates (note that only q^1_{on} and q^1_{off} are shown), but not for the transition rates, r_{on} and r_{off}. These observations for FL and ML-EM were generally true, as can be observed in Figure 4. Figure 5E shows the real time convergence distributions for neuron 1 for 100% and 400% initial parameter estimate perturbation cases under the same simulation conditions as Figure 4. For the FL and ML-EM algorithms, convergence was deemed to have occurred if, over 7.5 seconds of real time, all the parameter estimates remained within a deviation of 3%. It can be seen that the real times to convergence for ML-EM are approximately 2.0 to 3.6 times shorter than for FL. Note that, the benefits of the faster convergence of ML-EM than FL for the 400% initial perturbation case are negated by the poorer performance of ML-EM (see Figure 5B).

3.4 Three-Layer Network Simulations. To look at FL operating in larger networks and demonstrate the effects of FL estimation accuracy in one network layer on subsequent network layers, Figure 6 shows the estimation accuracy across the layers of the small and large three-layer networks described in the methods. Similar simulation settings as in Figures 4 and 5 are applied, with the exception that the initial transition and observation rate estimates are selected uniformly within the physiologically plausible parameter range. Figures 6A and 6B illustrate the distributions of the percent estimation error for r_{on} and r_{off} across the layers of the small three-layer network, respectively. By looking at the median values, it can be seen there is a slight increase in underestimation of the transition rates. Figure 6C shows the distributions of the percent estimation error for the

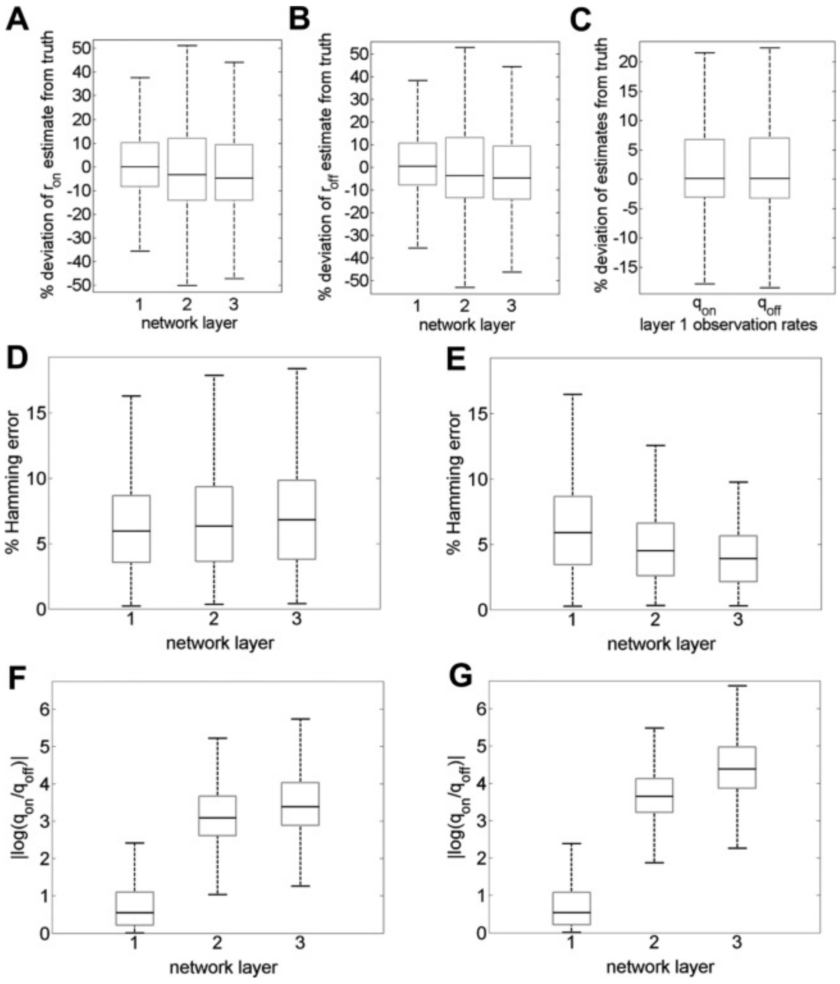

Figure 6: Three-layer feedforward network simulations using FL. The network layer 1, 2, and 3 distributions of percent parameter estimation error for (A) r_{on} and (B) r_{off} for the small network. (C) The layer 1 distributions of percent parameter estimation error for q^i_{on} and q^i_{off} for the small network. The layer 1, 2, and 3 distributions of percent Hamming error of the hidden state estimate for (D) the small network and (E) the large network with twice as many inputs in the higher layers. The layer 1, 2, and 3 distributions of informativeness for (F) the small network and (G) the large network. Data were collected over 1000 simulations lasting 10^6 time steps, where r_{on} and r_{off} are uniformly selected in the range of 1 to 115 s^{-1}, and the q^i_{on} and q^i_{off} are uniformly selected in the range of 1 to 1000 spikes/s. Initial parameter estimates were also selected uniformly in the same ranges.

observation rates for the neurons in layer 1 of the small network. As in the other figures, the median percent estimation error for the observation rates is small. Figure 6D shows the distributions of the percent Hamming error across the layers of the small network. There is a slight increase in the median percent Hamming error; however, this decoding error remains small at the final layer of the network.

Similar results are obtained when each unit in layers 2 and 3 pools over twice as many synaptic inputs; however, the increase in pooling leads to better decoding performance in layers 2 and 3. This can be seen by comparing the Hamming error in Figures 6D (small network) and 6E (large network with twice as many inputs in higher layers). The increased accuracy in the higher layers in the large network occurs because increasing the input to an adequate level provides a more informative level of evidence about the state changes.

An important property in layered networks is to recode relevant information in the inputs in a sparse manner with fewer output spikes at the top layers. This can be achieved with stronger synaptic weights at the higher layers. Here the informativeness of a given network layer is quantified by the distribution and median value of the final absolute value of the synaptic weights, $|\log(\hat{q}^i_{on}(t_f)/\hat{q}^i_{off}(t_f))|$, in the corresponding layer. Figures 6F (small network) and 6G (large network with twice as many inputs in higher layers) demonstrate that the informativeness of each network layer increases across the layers. Moreover, comparing Figures 6F and 6G indicates that doubling the number of inputs to the higher layers leads to more informative higher layers. This reflects the improved decoding performance of the large network with twice as many inputs in the higher layers.

To quantify the sparsity of spike coding, output spiking rates are estimated over the last 10^5 time steps of each simulation when learning has effectively stabilized. For the small three-layer network, although the median output spiking rate per neuron in each layer increases from layer 1 to layers 2 and 3 by 27.6% and 55.8%, respectively, the median total output spiking rate of each layer decreases from layer 1 to layers 2 and 3 by 38.5% and 64.3%, respectively. This indicates that fewer spikes are needed at the higher layers to encode the presence or absence of the input stimuli. Qualitatively similar changes were observed for the large three-layer network. The cost of spiking in higher layers can be reduced by increasing the spiking threshold g_o at each layer; however, for the case of FL-based learning, this needs to be traded off against parameter estimation accuracy as indicated in Figure 3L.

4 Discussion

We have demonstrated for a physiologically plausible range of parameters that FL is more computationally efficient than the benchmark ML-EM algorithm presented and also more robust when there is high uncertainty about the initial parameter estimates. The latter occurs because the ML-EM algorithm seeks out local maxima of the ML function and therefore typically will find local maxima rather than the global maximum when there is a large mismatch between the initial parameter estimates and the true parameter values. FL is a heuristic approach that seeks to count the number of state transitions and input spikes, determine the time spent in each state, and then estimate the BSN parameters. The FL estimation is robust to high uncertainty about the initial parameter estimates because the dynamic threshold enables estimation of the state even when the transition rate estimates are inaccurate (i.e., the resting potential of the log-odds ratio of the hidden state is offset from the true value) or when the synaptic rate estimates are inaccurate (i.e., synaptic weight magnitudes are not the appropriate size or sign). This is because the dynamic threshold fits to the short-term range of the log-odds ratio of the hidden state and, for the most part, can capture important log-odds ratio changes induced by input spike events regardless of their size or sign or the offset of the resting membrane potential or log-odds ratio.

It was observed that the computational run times for a fixed number of time steps are much longer for ML-EM than for FL, while the "real" (i.e., biological) time to convergence for the algorithms was shorter for ML-EM. This faster real time convergence for ML-EM, which can also be thought of as a more efficient use of the available data, may simply be due to the smoother convergence trajectory of ML-EM and the greater sensitivity of FL to fluctuations in the input statistics. It is also worth noting that these real convergence times are only approximate and primarily capture the times over which major estimate changes are taking place. Both FL and ML-EM can potentially give more accurate estimates if the simulations are run longer. Figures 5A and 5B show that FL estimates become more accurate for longer simulations. We did not consider longer simulations for ML-EM given that it becomes less tractable to complete a large number of simulations for different true parameter value combinations. The reason for the shorter computational run times for a fixed number of time steps of FL compared to ML-EM stems largely from the number of equations that need to be calculated by each algorithm at each time step. As the number of input synapses, N, increases, the number of equations grows more quickly for ML-EM than for FL. For FL and ML-EM, this number is $4N + 13$ and $28N + 6$, respectively. Although ML-EM appears to converge faster than FL (i.e., requires fewer time steps), the computational cost of ML-EM means that ML-EM still takes much longer to simulate to convergence than FL. Both the FL and ML-EM algorithms were implemented as sequential programs. For a single neuron, it would be possible to improve the computational efficiency of ML-EM compared to FL if multicore or GPU implementations were used. In particular, computations for the N synapses can be parallelized for both algorithms. Assuming full parallelization of the synapse computations and equations, this would effectively reduce the number of equations updated each time step to $4 + 13 = 17$ and $28 + 6 = 34$ for FL and ML-EM, respectively. Although this would improve performance for a single neuron, parallelization still consumes computational resources and therefore will provide a limitation of the size of the network that can be studied. Where only small networks are considered and computational resources are not an issue, FL would still be useful given its robustness to uncertainty in the initial parameter estimates.

The computational speed and robustness of FL indicate that it will be useful in studying hierarchical feedforward networks of BSNs within tractable simulation times. The study of larger networks is important for more complex inference problems such as feature and object recognition. Moreover, the simplicity of the FL algorithm means it is easier to take advantage of the spike coding efficiency of Bayesian spiking neurons in energy-efficient neuromorphic VLSI circuits compared to if online EM were to be implemented. The FL algorithm that we present is not necessarily intended to be biologically motivated, although its simplicity may make it computationally and mechanistically possible for real neurons to implement. Rather, the FL algorithm, which specifically applies to BSNs, represents a balance between simplicity and efficiency and provides a tool to study BSNs in greater detail in order to further understand their biological relevance and plausibility.

The study of larger networks is beyond the scope of this letter, but here we have considered the first step in this direction by simulating learning in a two-neuron network and in three-layer networks. Considering the two-neuron network, given the one input and a lower number of input spikes to neuron 2 compared to neuron 1, it was difficult for neuron 2 to accurately capture state transitions without the incorporation of the dynamic thresholds to estimate the auxiliary state. The dynamic thresholds thus enhance the stability and accuracy of the FL algorithm. Given that learning in BSNs is local to the neuron and here the FL algorithm appears stable over a large number of true parameter combinations, it is expected that the FL algorithm will be stable in larger networks, and this is supported by the simulations with the three-layer networks.

It is important to note that due to the symmetry of the HMM, although the FL algorithm can estimate the on and off parameters reasonably accurately, it cannot determine whether on is on or on is off. For example, the estimate $\hat{r}_{on}$ may be close to the true value for r_{off}, and vice versa. Thus, Figures 3 to 6 have been produced by checking if such parameter flips have occurred for both the FL and ML-EM algorithms. Although this may seem undesirable, the labeling of "on" and "off" is arbitrary and can be reversed without affecting estimation in the network.

It is also worth noting that given that the BSN spikes only when the hidden state is on (or off depending on how the parameters are defined or evolve), the learned observation and synaptic rates in the receiving neuron evolve such that the observation rate for the on state (q^i_{on}) takes a high value, while the observation rate for the off state (q^i_{off}) takes a value close to zero. This applies to both the FL and ML-EM algorithms and was observed for BSNs in feedforward networks that are not in the first layer of the network (not shown). To ensure this property did not affect the numerical stability of FL, very small observation rates were prevented (see section 2).

The ML-EM algorithm analyzed here (Denève, 2008b; Mongillo & Denève, 2008) is just one possibility; it may be possible to find faster online EM algorithms to estimate HMM parameters (Cappé, 2011) and many variants of online EM algorithms for HMMs exist (Krishnamurthy & Moore, 1993; Elliot, Aggoun, & Moore, 1995; Lindgren & Hoist, 1995; Le Gland & Mevel, 1997; Rydén, 1997; Stiller & Radons, 1999; Andrieu & Doucet, 2003; Tadić, 2010; Cappé, 2011; LeCorff & Fort, 2012). However, it is expected that FL will still be more computationally efficient because many of these methods aim for exactness of estimation, whereas FL focuses on the simplicity of the algorithm.

One possible shortcoming of the application of FL in hierarchical networks could be an accumulation of parameter estimation errors across layers of neurons. However, as is shown in Figure 6, the hidden state decoding performance can be reasonably stable, with median percent Hamming errors below 7% across the layers in the three-layer networks. Based on the results in Figure 3L, it may be possible in future versions of FL to control any under- or overestimation of parameters in subsequent layers by adapting the spiking threshold in each layer.

Perhaps the main shortcoming of FL is the dependence of estimation accuracy and bias on the range of the true parameters of the generative model. This is a reflection of the approximate nature of the FL algorithm. ML-EM, however, works for the full theoretically allowed true parameter range. Future work will be needed to find an FL variant that can improve this feature. Nevertheless, for a given problem, provided one knows what parameter range one is interested in, one can test FL for its estimation accuracy or bias on this parameter range. As is shown for a physiologically plausible parameter range, average FL-based estimation accuracy can be very good for an appropriately defined parameter range. Moreover, if FL is not very accurate over a certain parameter range, this may not be a significant problem because in many cases, approximate solutions may be adequate, and there will be high uncertainty about the true values of parameters, therefore limiting the accuracy of EM approaches, which can become trapped in local minima. On the other hand, FL gives a much more consistent parameter estimation regardless of the degree in uncertainty about the true parameter values. Moreover, the problems to which BSN networks can be applied are stochastic in nature, and thus small errors can be better tolerated.

An additional possibility, which reflects the complementarity of the FL and ML-EM algorithms, will be to first run the FL algorithm to get a reasonably small parameter estimation error and position the parameter estimates close to the optimum, and then apply ML-EM, which is more exact and has a better chance of finding the optimum if the initial parameter estimates are close to the true parameter values. These ideas should be the subject of future study, with a major aim of seeking to understand how neurons can perform probabilistic inference in sensory (Lochmann et al., 2012) and cognitive networks (Boerlin & Denève, 2011) and how such networks can efficiently learn to extract or integrate complex information about the external and internal environment.

Acknowledgments

This work was supported by the Australian Research Council Discovery Project grant DP1096699 and the University of Western Sydney.

References

Andrieu, C., & Doucet, A. (2003). Online expectation-maximization type algorithms for parameter estimation in general state space models. In *Proceedings of the Int. Conf. Acoustics, Speech and Signal Processing* (vol. 6, pp. 96–72). Piscataway, NJ: IEEE Press.

Barber, M., Clark, J., & Anderson, C. (2003). Neural representation of probabilistic information. *Neural Comput.*, *15*(8), 1844–1853.

Boerlin, M., & Denève, S. (2011). Spike-based population coding and working memory. *PLoS Comput. Biol.*, *7*(2), e1001080. doi:10.1371/journal.pcbi.1001080

Cappé, O. (2011). Online EM algorithm for hidden Markov models. *J. Comput. Graph. Statist.*, *20*(3), 728–749.

Denève, S. (2008a). Bayesian spiking neurons. I: Inference. *Neural Comput.*, *20*, 91–117.

Denève, S. (2008b). Bayesian spiking neurons. II: Learning. *Neural Comput.*, *20*, 118–145.

Elliot, R. L., Aggoun, L., & Moore, J. B. (1995). *Hidden Markov models: Estimation and control*. New York: Springer.

Knill, D., & Richards, W. (1996). *Perception as Bayesian inference*. Cambridge: Cambridge University Press.

Kording, K., & Wolpert, D. (2004). Bayesian integration in sensorimotor learning, *Nature*, *427*, 244–247.

Krishnamurthy, V., & Moore, J. B. (1993). On-line estimation of hidden Markov model parameters based on the Kullback-Leibler information measure. *IEEE Trans. Sig. Process*, *SP-41*, 2557–2573.

Kuhlmann, L., Hauser-Raspe, M., Manton, J., Grayden, D. B., Tapson, J., & Van Schaik, A. (2012). Online learning in Bayesian Spiking Neurons. In *Proceedings of the 2012 International Joint Conference on Neural Networks (IJCNN).*

Le Corff, S., & Fort, G. (2012). *Online expectation maximization based algorithms for inference in hidden Markov models.* arXiv.org, vol. math.ST. arXiv:1108.3968v2.

Le Gland, F., & Mevel, L. (1997). Recursive estimation in HMMs. In *Proc. IEEE Conf. Decis. Control* (pp. 3468–3473).

Lindgren, G., & Hoist, H. (1995). Recursive estimation of parameters in Markov-modulated Poisson processes. *IEEE Transactions on Communications*, *43*, 2812–2820.

Lochmann, T., & Denève, S. (2008). Information transmission with spiking Bayesian neurons. *New J. Phys.*, *10*, 055019.

Lochmann, T., Ernst, U. A., & Denève, S. (2012). Perceptual inference predicts contextual modulations of sensory responses. *J. Neurosci.*, *32*, 4179–4195.

Mongillo, M., & Denève, S. (2008). Online expectation-maximization in hidden Markov models. *Neural Comput.*, *20*, 1706–1716.

Rabiner, L. R. (1989). A tutorial on hidden Markov models and selected applications in speech recognition. *Proceedings of the IEEE*, *77*, 257–286.

Rydén, T. (1997). On recursive estimation for hidden Markov models. *Stochastic Processes and Their Applications*, *66*(1), 79–96.

Stiller, J. C., & Radons, G. (1999). Online estimation of hidden Markov models. *IEEE Signal Processing Letters*, *6*(8), 213–215.

Tadić, V. B. (2010). Analyticity, convergence, and convergence rate of recursive maximum-likelihood estimation in hidden Markov models. *IEEE Trans. Inf. Theor.*, *56*, 6406–6432.

Zemel, R., Dayan, P., & Pouget, A. (1998). Probabilistic interpolation of population code. *Neural Comput.*, *10*(2), 403–430.

Received September 7, 2012; accepted October 9, 2013.